Machined surfaces as designed cell culture substrates

Kunal Sharma

2021

LUND UNIVERSITY

LTH
FACULTY OF
ENGINEERING

Author: Kunal Sharma
Lund, Sweden 2021

Avdelningen för Industriell Produktion
Lunds Tekniska Högskola
Lunds universitet
Box 118
221 00 Lund
Sverige

Division of Production and Materials Engineering
LTH, School of Engineering
Lund University
Box 118
SE-221 00 Lund
Sweden

Foreword

With constantly changing regulations around the current COVID-19 pandemic, obtaining access to all the laboratories was a real challenge. This resulted in smaller sample sizes, and less overall experimentation than originally intended by the author.

However, this thesis process was made very enjoyable, thanks to Filip Lenrick and Martin Hjort and their continued support, supervision, and occasional casual ZOOM meetings. Thank you to Mikael Hörndahl for his guidance in sample preparation, and Daniel Johansson from SECO Tools AB for their assistance in tool selection and believing in this project. As well as everyone at the Division of Production and Materials Engineering for their education and moral support throughout this entire Master's process.

Thank you too all the friends that were always ready with distractions, the Brunch Squad for tasty meals, Malmö Roddklubb for the much-needed mental breaks, and Shao Du for being the hardest working Master's thesis student trying to encourage focused writing times even during the rare sunny weather.

Finally, to my family who is always there behind the scenes helping with the hard decisions and making sure I make good choices for the majority of the time.

Lund 2021-06-01

Kunal Sharma

Sammanfattning

De flesta levande celler fäster på ytor av olika slag för att kunna växa, men vilka faktorer som bidrar till deras infästning på metallytor är hittills okänt. Man vet att ytans ojämnhet spelar en roll och att vissa material är cytotoxiska. Målet med den här studien är att vidare undersöka effekten som ojämnheten har på cellproliferation, genom att odla celler från cellinjen A549 på olika metallytor. Metallerna som undersöktes var Ti6Al4V, Ti Grade 2, Ti Grade 11, Al 7075, CW510L, AZ31, och AZ61a. Förhoppningen är att överbrygga klyftan i det nuvarande kunskapsläget vad gäller ojämnhet och att etablera ytor bearbetade för cellodling, genom bl.a. fräsning, och därigenom minska både materialkostnader och tiden det tar att förbereda prover. Ojämnheten på metallerna som undersöktes i studien var mellan $0.5 - 0.14$ µm. Cellerna räknades genom att analysera bilder tagna med svepelektronmikroskop. Den högsta cellproliferationen observerades vid analys av areafraktioner vid en ojämnhet på ca 0.15 µm (R_a). Metallproverna jämfördes med en kontrollgrupp som bestod av glasskivor, vilka för närvarande är allmän praxis att använda vid cellräkning. Alla prover (AZ31, Al 7075, och Ti6Al4V) förutom CW510L visade efter fräsning bättre resultat än kontrollgruppen. Studien beskriver ett lämpligt arbetsflöde för framtida undersökningar av cellproliferation på ytor av metall. Den etablerar även de aktuella metallerna och deras egenskaper vad gäller ojämnhet som optimala för framtida tester, för att så småningom utveckla nya alternativ till implantat att använda i människokroppen.

Nyckelord: Yttopografi, cellproliferation, celladhesion

Abstract

Most living cells attach and proliferate on surfaces, but the reasons for attachment are scarcely researched when it comes to attachment on metal surfaces. Surface roughness is known to have an effect, and some materials are known to be toxic to cells. The aim of this study is to further investigate the effects of surface roughness on cell proliferation through the use of the A549 cell line planted on metallic surfaces. The metals investigated in this study are: Ti6Al4V, Ti Grade 2, Ti Grade 11, Al 7075, CW510L, AZ31, and AZ61a. The study hopes to bridge the current gap in the scope of surface roughness investigations. As well as to establish machined surfaces i.e. through milling operations as an option for cell culture substrates. Thus, reducing both costs of materials, and the time for sample preparation. The investigated range of surface roughness values was between 0.5 – 0.14 µm. The cells were counted using image analysis of images obtained from the scanning electron microscope. The highest cell proliferation was seen through area fraction image analysis at approximately 0.15 µm (R_a) surface roughness. The metal samples were compared to a control group, in this case being glass slides currently common practice for cell counting. All the samples (AZ31, Al 7075, and Ti6Al4V) except for CW510L performed better than the control group after undergoing milling operations. The study outlines a suitable workflow for future evaluation of cell proliferation on metal surfaces. This further establishes these metals and their surface roughness conditions as optimal for future testing and development to ultimately achieve new options to be used as implants in the human body.

Keywords: Surface topography, cell proliferation, cell adhesion

Table of Content

List of Figures

1. Introduction

1.1. Background

Certain living cells can attach in a plethora of different ways to various surfaces depending on their geometry and surface chemistry. Understanding cell response and proliferation based on material surfaces is vital for various fields of research ranging from clean water supply to implants inside the human body [1]. In this area of research, a lot of experiments have been done both *in vitro* and *in vivo* to investigate the physical and chemical properties that affect cell proliferation [2-5]. Different environments or products either cause cells to thrive, or stunt proliferation. In clean water supply piping for example the goal is to not allow for any cell attachment, especially fungi. On the other hand, biocompatibility is crucial for body implants, or any other foreign objects implanted in humans or animals. Keeping this in mind research over the years has focused on identifying materials for both applications [4, 6-8]. A study by Grill *et al.* considered six single phase metals alloys and investigated their ability for cell proliferation [5]. This base study considered *in vitro* testing due to the possibility for inflammation in the body if *in vivo* studies were conducted. This move to *in vitro* testing was a common trend in the 1990's due to the developed ability for cell proliferation testing *in vitro* which allowed for more diverse experimentation, with more robust cell lines, and more repeatable experiments.

Very little is known about cell growth and attachment onto machined surfaces. Majority of the researched cell attachment on metals is done through very precise sample preparation in the hopes of achieving specific surface roughness [1]. This study will explore a range of surface roughness values and material types to see how living cells react to the different conditions. One of the main benefits of this study is the juxtaposition of metal samples that are prepared through grinding, which is the current practice and samples that undergo a milling operation which yields results in a shorter time frame without sacrificing cell proliferation qualities. Combining machining and life sciences in this way would allow for a collaboration that would result in quicker and more cost-effective solutions by performing direct experiments on metal surfaces.

1.2. Aim

This study focuses on two main aims: to establish the experimental setup, and to develop cell proliferation testing by utilizing simple machining processes. With a goal to establish an efficient workflow for determining metal biocompatibility and streamlining the process of discovering possible materials for implants. A more detailed description is listed below:

1. Investigate the surface roughness effects on cell proliferation in order to determine the optimal surface roughness range for attachment. This will also confirm the previously known conclusions from currently published articles and show reproducibility of results.

2. Determine the cell proliferation based on the chemical composition of the various metal samples, after undergoing the same machining process. This will also support the goal of establishing simple machining processes as an option for cell proliferation investigations.

1.3. Previous applications

The range of cell proliferation experiments on metal surfaces is vast, ranging from golden dental implants to titanium bone implants. There have been studies performed investigating the cell attachment on steels which are currently used in orthodontic applications, and copper ions released in prosthetic materials which are predominantly cobalt alloy based which stunt cell proliferation [8]. Woodman *et al.* explored the titanium alloys as implants in baboons and noticed that the lungs and spleen contained higher than normal levels of titanium [9]. Over time these *in vivo* tests were suspended due to the unnecessary use of animals. More and more animal testing moved to *in vitro* testing since methods for cell proliferation *in vitro* were more developed and allowed for more rigorous and repeatable experimentation. Another major advantage is the fact that with *in vitro* testing the cell lines are technically infinite. The cells can be cultured up to the required density (cells/cm^3) and a portion of them can be set aside for more proliferation for the next experiment [11]. The only limiting factor for cell line experimentation seems to be time, and the fact that for biocompatibility some of the tests require for *in vitro* testing at later stages before the materials are approved for human compatibility.

2. Relevant Theory

This section dives deeper into the currently known theory surrounding cell proliferation on metallic surfaces, milling and grinding operations, cell culturing, scanning electron microscopy (SEM), and Optical 3D microscopy, which are all utilized in this study. Majority of the cited papers deal with cell proliferation with the goal of identifying bio-compatibility. The following sub-sections are broken down into more digestible volumes, the sub-sections build-up to accommodate the reader's understanding of the following sections in this study as well as identifying key characteristics affecting experimental setup and results.

2.1. Physical & chemical properties

A substantial amount of research has been conducted in biomaterials used in tissue engineering or implant technology [1, 5, 8, 10], very few experiments have been performed using less specialized metals such as; iron, aluminum alloys, carbon steels, and brass. This is generally due to their toxicity or poor corrosion properties. There is a good understanding in this field of research that the physical and chemical properties of the material surface are related to cell proliferation [2, 4, 10-12]. Huang *et al.* in their study [11] have found that an arithmetical mean surface roughness value (R_a) of 0.15 µm is optimal to achieve the highest proliferation rate of osteoblast-like cells in Titanium (Ti) surfaces. The range of R_a values investigated was from 0.05-1.20 µm. These results suggest that cell attachment happens most successfully neither at the roughest or smoothest end of the spectrum. Investigating this specific range of surface roughness values allowed Huang *et al.* to determine this bell-shaped curve, which can be seen in Figure 1 labelled as areas I and II.

However, since the range of selected roughness values is between 0.15-1.20 µm, it was interesting to see what effects a larger surface roughness range could have. One of the topics investigated was to determine whether this trend persists at a wider range of roughness values. Keller *et al.* concluded that a rougher surface (sandblasted) experienced an order of magnitude more percent cell attachment when compared to the smooth (1 µm diamond paste polished) surface [10]. This was combined with the conclusions of Huang *et al.* in Figure 1, where III shows Keller *et al.*'s experienced trend. It should be mentioned though that Keller investigated the cell attachment after 1h of exposure. In this case the roughest end of the spectrum resulted in the best results. This could potentially lead to opposite findings, where the previously found bell curve would instead show a U-shaped curve. This trend would

have the most cell attachment at the smoothest, and roughest ends of the spectrum with less attachment in the middle. This would rather suggest that there is a local minimum present when it comes to surface roughness values and their effects on cell proliferation. This trend can be seen in Figure 1 below. Chung *et al.* concluded that from a nano-scale perspective an increase in surface roughness lead to better cell attachment which is symbolized as I in Figure 1. On the other hand, [2] has shown opposite findings, where a smoother surface has led to a higher initial adhesion as well as a more increased spreading on the surface. This poses the question, as to whether cell proliferation should only be counted in terms of cell density, or if types of attachment should also be investigated. Lange *et al.* found that the cells attached within the grooves for machined samples mainly [12]. Therefore, in this study the machined samples will be evaluated based on both cell density, and the type of attachment.
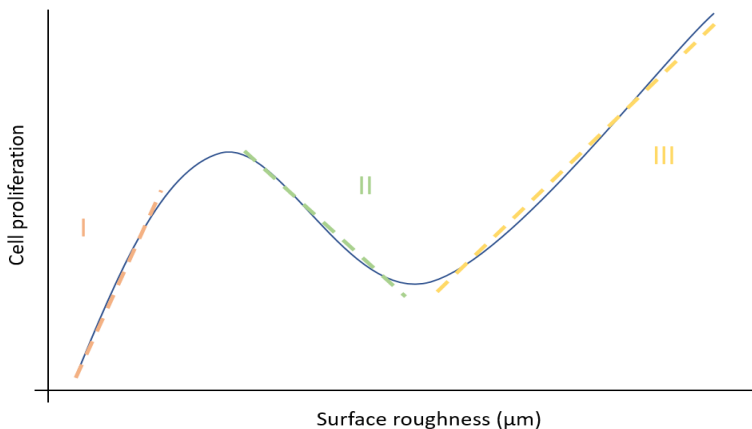
Figure 1: *The three experienced surface roughness effects based on the investigated literature currently conducted in the area of cell proliferation*

2.1.1. Cell attachment types & orientation

Lange *et al.* in their study noticed a pattern for the rougher surfaces, where some of the cells would attach within the valleys, and some cells chose to bridge the valleys [12]. Unfortunately, the surfaces were not unidirectional so conclusions could not be drawn as to whether the cells have a preference. In another study, by Wen *et al.* they noticed that the surface roughness of the sample affected whether or not the cells had a preferred orientation and type of attachment [13]. At rougher surface values the cells seemed to not have a

preferred orientation, and these results could only be seen after 24h of exposure. At lower surface roughness values the directionality of cell proliferation is lost.

For simplicity purposes this study modified all the silicon-carbide (SiC) grinding paper values into the FEPA P system provided by Struers [14]. On the other hand, the opposite results were seen by Anselme *et al.* in their study where the samples prepared with P4000 and above SiC grinding paper resulted in no apparent cell preferred orientation [2]. Figure 2 (a) shows the cell attachment tendencies based on a study by Huang *et al.* which suggests that cells have a preferred proliferation direction based on the surface properties. The values for grain size and comparison to the America National Standards Institute (ANSI) is adapted and provided in Appendix A - Grinding grain size values for FEPA P-scale adapted from [14].
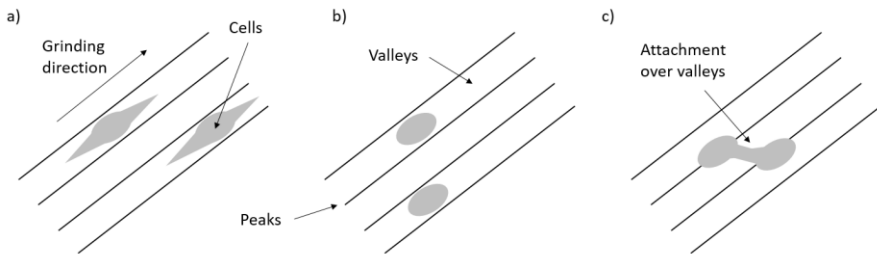
Figure 2: *Cell attachment locations and types based on observations made in [11] and [12]. (a) shows directionality of cell proliferation, (b) attachment within valleys, (c) the bridging attachment over valleys*

A study by Lange *et al.* demonstrated that cells preferred attachment within the valleys for machined surfaces, however attachment over valleys was present on smoother surfaces [12]. Cell proliferation times varied largely amongst the different experiments, the most common ones being 24h or 48h for relevant experimental goals [11, 15, 16]. One of the main reasons for early experiment termination is to avoid the over-crowding of cells, more commonly referred to as confluency.

2.1.2. Metal specific properties

This sub-section discusses the currently known advantages and disadvantages of some of the metals that will be used in this study. The purpose is to provide some background knowledge into the common trends within these metal family groups.

2.1.2.1. Tantalum

Tantalum (Ta) is a metal used in this study which has recently gained popularity in the field of orthopedics, however the interaction between the metal and cells has scarcely been researched. Findlay *et al.* focused on identifying cell attachment and morphology when exposed to Tantalum and compared their results to more common materials such as titanium, cobalt-chromium alloy, and tissue culture plastics [17]. Cell attachment was measured by comparing attached cells as a fraction of total cells added at 30min, 1h, and 2h. The number of cells added was $2 \cdot 10^4$. At each time point the unattached cells were washed off with a phosphate buffered saline (PBS) solution, the remaining cells were stained with crystal violet and counted. What was concluded was that the surface roughness did not play a role in cell proliferation for the Ta samples. This is opposite to previous trends found on other metal surfaces where the cells had a preference within a specific surface roughness range [10].

2.1.2.2. Magnesium alloys

Magnesium (Mg) alloys are generally not used as biomaterials due to their poor corrosion properties [18]. However, they have many advantages such as; similar to bone density, they are readily available, have high specific strength even when compared with Ti6Al4V. Li *et al.* investigated the cytotoxicity of magnesium and concluded that there were no inhibitions in cell proliferation with regards to their exposure to magnesium alloys. These results are promising and the corrosion concerns were addressed by suggesting the use of heat-treated magnesium alloys which exhibited better corrosion properties than the pure untreated samples [19]. Lastly, a study by Gu *et al.* concluded that magnesium with alloying contents of aluminum (Al), tin (Sn), and zinc (Zn), improved corrosion properties and had no negative impacts on cell proliferation [20]. For this study two magnesium samples are considered AZ61a, and AZ31. AZ61a contains some silicon (Si) which should perform worse than its relative AZ31, based on previous conclusions and research.

Craig *et al.* in their study found that the high biocompatibility of gold (Au) and palladium (Pd) was most likely due to their nobility, whereas the biocompatibility of Ti was suggested to be related to the formation of a highly adherent TiO_2 layer [4]. This trend regarding cell proliferation due to a strong oxide layer could also be present in the Mg-alloys.

2.1.2.3. Copper

A lot of research on the chemical properties of metal samples has been conducted in the dental industry. One of the most prominent studies was by Grill *et al.* in their paper about the influence that metal alloys in dental implants have on cell proliferation [5]. The study found that (Au) is effective in maintaining cell viability [4] when combined with other alloying elements as long as the content is above 71 weight percentage (wt.%) [8]. Through cell culture tests Craig *et al.* experimented on 29 alloys, and 6 pure metals. The pure metals are of special interest to this study and those were: Au, Pd, Ti, silver (Ag), nickel (Ni), and copper (Cu). The metals were ranked based on various criterions i.e. optical density, and visual ranking of the stain intensity. They concluded that Au, Pd, and Ti were least cytotoxic, and Cu ranking last meant highest cytotoxicity when compared with the other pure metals [4]. This concept is well known nowadays, which can be seen in currently developed dental implants which all have low to zero concentration of Cu. An interesting concept that this thesis study will investigate is whether in a Cu-rich environment cells have a preference of attachment. When considering brass and the different Cu-rich phases within brass it will be interesting to see which phases the cells are most attracted to, or if all of them are equally toxic to cell proliferation.

2.2. Milling

Milling operations were carried out with a tool provided by SECO Tools AB in order to demonstrate the ability of cell proliferation on machined surfaces without the need for extensive sample preparation through grinding. The tool holder product number is: R217.69-2532.0-06-8AN, and the tool insert: XOEX060204FR-E03 H15 was used. The specifications for the tool insert can be found in Appendix B- SECO tool insert. The tool holder, and insert were selected based on the hardest milling operation in terms of highest forces which would be present during the machining of Ti6Al4V. The tool holder and insert were recommended by SECO Tools AB based on the machining requirements.

2.2.1. Wear mechanisms

Based on the metal cutting theories and models textbook by Ståhl *et al.* [21] wear leads to geometric changes in the cutting tool, which are a result of multiple types of wear i.e. abrasive wear, adhesive wear, diffusion wear, and chemical wear. These types of wear result in geometric changes such as flank

wear, crater wear, and notch wear. Figure 3 shows the areas and results of the different types of geometric changes due to wear.
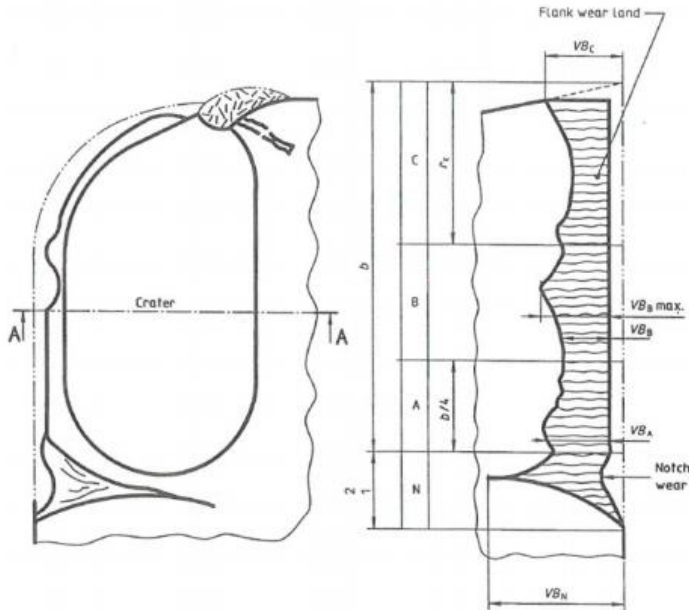
Figure 3: Crater wear and flank wear illustrated, to identify the typical areas for wear, and their characteristics, adapted from [22]

Flank wear is seen on the surface parallel to the workpiece cutting operation, and is used as a criterion for tool life, in most cases. Excessive flank wear could lead to the bending of the tool since the edge line shifts in regard to the workpiece resulting in higher forces being experienced [21]. Crater wear is more prominent on the rake face and results in micro-welding or adhesion of material on the cutting face of the tool. This would result in the weakening of the cutting edge due to the decrease in thickness which could result in plastic deformation and eventually cracking. As well as leading to a more positive rake angle [21]. Lastly, notch wear is generally the result of high temperatures and oxidation that happens on the clearance face of the cutting tool. More specifically the point at which the chips lose contact with the cutting tool. The high temperatures trigger oxidation which results in wear increasing in that area [21]. Oxidation has been found to occur more rapidly in intermittent cutting operations due to the short periods of exposure to the outside environment [21]. The outside environment in this case is the area outside of the cutting zone. Another factor that could lead to notch wear is

the work hardening of the outer layer of the workpiece which is done through multiple cutting operations [21].

2.3. Grinding

Grinding is common practice for almost all produced or manufactured parts accounting for 20-25% of machining costs [23]. A grinding paper consists of hard particles in a bonding matrix. For this study SiC grinding paper was used with varying grits ranging from P220 to P4000. The problem with grinding operations is the unpredictable nature of the cutting process that occurs since each grain particle acts as a tool. The grains are not only randomly spread out on the grinding paper, they are also randomly orientated [23]. Due to the difference in hardness between the grains within the SiC paper and the particles in the metal samples used, the amount of material removed varies largely. From theory it is also know that the difference in hardness results in different tool degradation to be experienced by the SiC paper leading to a different tool life time [21]. If we consider a surface grinding operation with automatically rotating samples on top, which was used for this study. The force with which the samples are loaded would have to vary based on the amount of material that has to be removed in one rotation. Secondly, the time for grinding would vary in order to control the overall amount of material removed. This variability in the reproducibility of results makes grinding an unpredictable operation. This leads to constant inspection of the surface roughness in order to determine whether more grinding is necessary. This study also hopes to provide a simple generic model for achieving a specific surface roughness through grinding. However, this will be limited to only the materials that were used.

2.4. Surface roughness

Two types of surface roughness values were recorded in order to have a valid comparison and try to disregard the effects of skewness. The two types of roughness considered were arithmetical mean roughness (R_a), and the total height (R_t). This was done based on previous experiments conducted by Anselme *et al.* and their method [2] that measured 6 3D images for each sample and without filtering, computed the R_a and R_t values. The value of R_a would be used to evaluate the overall deviation in the surface roughness. It will be used as the main comparison between samples. R_t will be used as an additional comparison to exemplify the total range between the minimum and maximum value of surface roughness achieved from the profile

measurement based on the 3D optical constructed image from optical microscopy.

2.4.1. Arithmetical mean roughness value

To calculate the R_a value the absolute values of the profile roughness are considered based on the deviation from the mean roughness value. The absolute values of deviation are then averaged to provide the R_a value [24]. The inverted absolute value peaks can be seen in Figure 4.
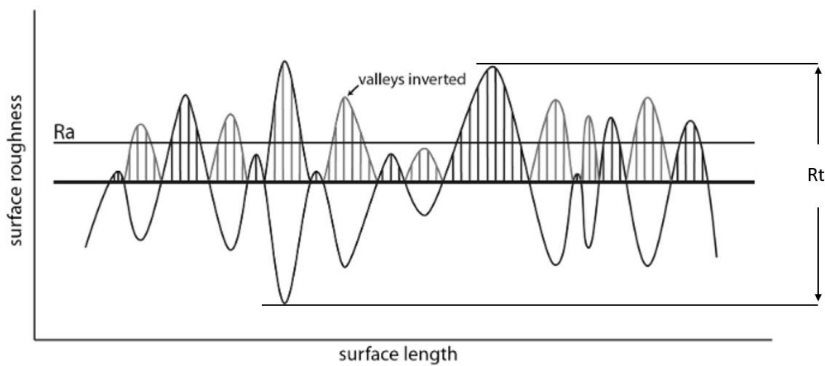
Figure 4: Measurement steps for determining R_a and R_t values based on a surface profile measurement, adapted from [25]

2.4.2. Total height of the roughness profile

The R_t value is simply the distance between the largest valley and the tallest peak, as seen in Figure 4 [24]. This value is useful in order to see the two extremes and to understand that range within which the surface roughness exists, although it may not be characteristic of the entire surface. If there is preferred cell attachment in specific areas due to the roughness values these could be explained by the R_t value which capture the entire range rather than a mean value.

2.4.3. 3D optical microscopy

ALICONA Infinite Focus microscope was used to create a 3D surface roughness measurement. The measurement is taken by recording multiple images and splicing them together over a short height distance. This allows

the microscope to build a 3D height image since the focus shifts to different surfaces with the change in height. This method of microscopy is known as focus variation microscopy [25]. A magnification of X20 was used for all measurements and images. The field of view analyzed was approximately 500 µm x 500 µm.

2.5. Cell culturing

Cell culturing is generally done using either primary cells (taken from a host), or cell lines which are immortalized primary cells that exhibit specific properties. The cell lines are derived from primary cells and are considered to be more robust, survive longer, and carry less biological variability [26]. Since over time *in vivo* testing raised ethical dilemmas resulting in the cost of experiments to go up. More and more tests nowadays use cell lines in less critical studies or pilot programs [16]. These so-called *in vitro* tests allow for cell culturing until the cells have proliferated to a certain density (cells/cm^3), i.e. number of cells per milliliter which is then used to conduct experiments.

The cell lines are kept in flasks with medium, for this particular experiment the medium used was the so-called F-12K which is a sugary solution. The medium is supplemented with 10% fetal bovine serum, which supplies essential proteins to allow for cell growth, and 1% penicillin/streptomycin which is an antibiotic to reduce the risk of contamination. The medium is also supplemented with the pH sensitive dye phenol red which is an easy-to-observe indicator about culture quality. Contamination would be the result of a bacterial or fungal infection which would require the cells to be discarded, and for the incubator and cell culture hood to be thoroughly sterilized. It is possible to try to remove the contamination through a series of steps however, this is reserved for critical cells [26]. In this experiment the cells used are not considered critical, therefore culturing new cells would be easier. Proper aseptic culture protocols, such as ample decontamination using 70% EtOH minimizes the risk of contamination.

2.5.1. Incubation

In order to allow for cell proliferation and division they must be incubated in specific conditions. These conditions are maintained to keep the cells alive, and they consist of three main components, temperature, humidity, and CO_2 concentration. The time for incubation varies largely amongst different experiments in the related area of cell proliferation on metal surfaces, ranging from anywhere between 1h to 72h [10]. For this particular set of experiments

the cells were incubated for 48h in 37 ºC, 90% relative humidity, and 5% CO_2 concentration, similar conditions were used in [27] which seems to be common practice in these types of experiments.

2.5.2. A549 Cells

The A549 cell line was used for *in vitro* testing of the metal samples in this study. The A549 is a human lung adenocarcinoma cell line [28]. They were chosen due to their robust nature, ease of culturing, and adherent nature. The main criterion for selecting the cells was that they had to be easily cultured, and not too sensitive to the environment to allow for inspection over a longer period of time.

2.6. Scanning Electron Microscopy

Utilizing a scanning electron microscope (SEM) is not common practice for cell culturing experiments, however due to the non-transparent nature of metals it was necessary for cell counting. A focused beam of electrons is scanned across the surface of the sample and the supporting detectors build the image based on electron interactions. The samples used are all flat polished, and electrically conductive allowing for easy SEM imaging [29]. The emitted electron beam energy range used in this study is between 10-20kV which allows for an inspection of properties at different depths of the sample and a greater volume of inspection overall. Figure 5 illustrates the detector positions for secondary electrons (SE), backscatter electrons (BSE), and X-ray energy dispersive spectroscopy (XEDS), as well as the different escape depths for the different techniques. This could be done for example when oxidizing layers develop and the area of interest happens to be below the oxidizing layer. A higher voltage allows for a deeper penetration. Using a SEM allows for the inspection of the material composition, topography, and microstructure [29]. This study focuses on the identification of cells which are carbon based, as well as determining the preferred attachment sites for the cells based on known chemical and physical properties.
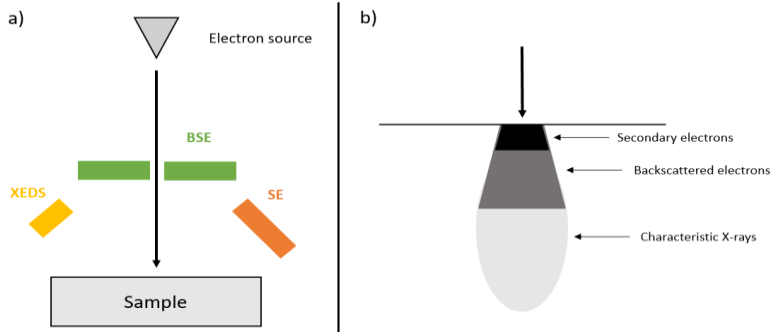
Figure 5: Simple sketch describing SEM operation; (a) detector placements for SE, BSE, and XEDS, (b) escape depth of the different signals

2.6.1. Secondary electrons

Figure 6 shows the different types of electron scattering. For SE the emitted electron beam with a high enough intensity would inelastically scatter and knock-out the present valence electrons within the atom. Bright spots in SE images signify the location of tall objects, these are generally highly charged which results in the visual bright spot [29, 30]. The SE images are used more for surface analysis, they are the starting point to determine the area of interest and where to focus for BSE investigation.
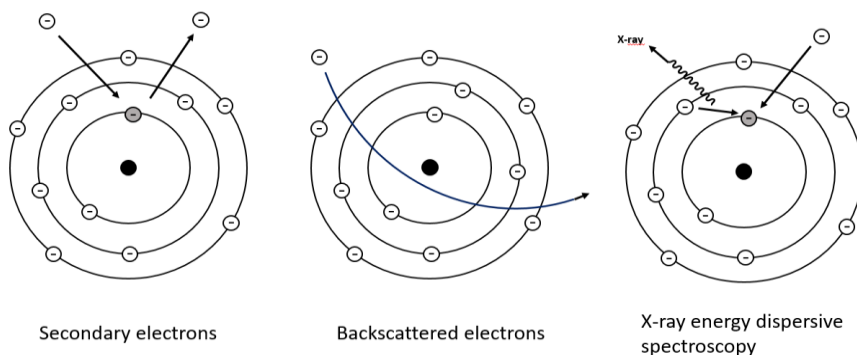
Figure 6: Scattering of electrons illustrating the difference between SE, BSE, and XEDS

2.6.2. Backscattered electrons

BSE are electrons from the incident beam that underwent elastic scattering and were able to return back up towards the source. The BSE detector surround the beam source opening in order to detect these electrons. The BSE are used to determine various compositions and precipitates within the material allowing for an illustration of an alloying element. Using the BSE, allows the user to see heavier atomic number components which appear brighter in the generated image. This is due to the higher nuclear mass of the higher atomic number elements. They elastically scatter the incident beam however low atomic number elements have less nuclear mass thus limiting this phenomenon resulting in a darker image region appearance on the generated images [29, 30]. Figure 6 illustrates the elastic scattering of the incident electrons that are detected using the BSE detector. Therefore, if the primary goal is to identify carbon-based cells, they would be resolved counted easier when contrasted with heavier atomic number elements in the background for example Ti, V, Cu, or Zn.

2.6.3. X-ray energy-dispersive spectroscopy

X-ray photons are emitted by the sample during inelastic scattering of the incident beam electrons. These X-rays are generated by the electrons jumping between different electron shells, which is the result of electron displacement and inner shell ionizations from the incident beam. To achieve this the incident electrons must possess a higher energy than the electron binding energy of the elements. These emitted X-rays from electron shell jumps are characteristic to specific elements. This method allows for the detection and quantification of elements present within the sample [29]. XEDS will be utilized to determine the presence of carbon-based cells, and the area where the cells tend to migrate towards.

3. Experimental methods

This section is divided into three major sub-sections; surface preparation, cell deposition, and quantification.

3.1. Surface preparation

Disks of metals and metal alloys were prepared with dimensions of 20-23mm diameter. They were used for testing as-purchased from the manufacturer. 3 samples were made from each material in order to:

1. Grind the sample to a specific surface roughness

2. Mill the surface with the SECO milling tool

3. Perform hardness testing

After machining the surface roughness R_t and R_a were recorded for all samples using optical 3D microscopy.

3.1.1. Sample composition

Table 1 describes the composition of the samples used in this study. These elements are used for XEDS tracking to determine if the cells have preferred areas of attachment.

Table 1: *Metallic sample compositions for Ti6AL4V[31], AZ31 and AZ61a [32], Al 7075 [33], CW510L [34], and Ti Grade 2 [35]*

Sample	Composition (wt. %)				
Ti6Al4V	Al	V	C	Fe	Ti
	5,48	4,22	0,369	0,112	Balance
AZ31	Al	Zn	Mn	Si	Mg
	3,1	0,73	0,25	0,02	Balance
AZ61a	Al	Zn	Mn	Si	Mg
	6,2	0,74	0,23	0,04	Balance
Al 7075	Zn	Mg	Cu		Al
	5,6	2,5	1,6		Balance
CW510L	Cu	Pb	Fe	Sn	Zn
	57,46	0,1	0,0342	0,0058	Balance
Ti Grade 2	Fe	O	C	N	Ti
	0,3	0,25	0,1	0,03	Balance

3.1.2. Machining

The metals underwent multiple machining steps, starting with either turning (AZ61a, AZ31, CW510L, and Ti6Al4V), or stamping (Al 7075, and Ta 99.9% purity). Lastly, Ti Grade 2 was sawed from a hollow tube. All samples went through two finishing processes either grinding for specific surface roughness targeting, or milling with the use of the SECO tool.

3.1.2.1. Turning

Turning operation were performed in two main stages, roughing to turn down the stock to the required diameter of 20-23mm, and parting. The parting operation consisted of facing the front end of the sample, then parting the disk at a thickness of 2mm repeating these steps 3 times. Each of the 3 samples within each material group would have a specific task.

3.1.2.2. Grinding/Polishing

Before the samples could be grinded/polished they had to be imbedded into a resin to allow for easier sample handling and a stable base. This was done using the Struers CitoPress machine with the MultiFast resin. Table 2**Error! Reference source not found.** explains the setup used for resin curing.

Table 2: MultiFast resin curing procedure setup

Resin (ml)	Time (min)	Temp (°C)	Pressure (mbar)	Cooling (min)
20	3	180	300	2

The grinding process used in this experimental process was surface grinding using the Struers Tegramin 30 grinding machine. The setup for grinding had to vary based on material hardness, to allow for proper surface roughness targeting. Appendix C - Grinding conditions for sample preparation provides the overall setup for grinding for each of the metallic samples. Between each of the changes of the SiC paper grits the samples were washed with water and dried with pressurized air. After the final grinding step, the samples were washed with ethanol in an ultrasonic bath for 5min using the BRANSON 2510. The samples were then wrapped in ultra-fine long-fibered paper towel to prevent any scratches and contamination.

3.1.2.3. Milling

One sample from each metal group underwent a milling process with the SECO tool. The cutting data used was the same for all samples: 560RPM, 55 mm/min feed, and 0.05 mm depth of cut. The tool was used with only one insert to allow for a coherent surface finish. Wiper technology was considered for a better surface finish, the provided tool had a wiper edge length of 1.1mm which can be found in the product description illustrated in Appendix B- SECO tool insert. The same insert was used for all metal samples to see the amount of wear present after sample preparation, further analysis can be found in Results & Discussion.

3.1.3. Hardness testing

The hardness testing was performed using the Vickers hardness scale for all the metal samples. The Vickers scale is based on a diamond indenter that is pressed into the material with a force of 10 kg, and a dwell time of 15 seconds. To measure the hardness value Equation 1 is used, where P is the load in N, and d_1 is the average of the two diagonals created by the indenter [36].

$$HV = 1.854P/d_1^2 \hspace{4cm} \textit{Equation 1}$$

3.1.4. Optical microscopy

ALICONA InfiniteFocus (IF) was used for 3D optical microscopy of the surfaces that were generated from grinding and milling. The surface roughness values of R_a and R_t were recorded using the ALICONA IF-MeasureSuite. Since the samples were already immersed in resin, they had a flat surface to stand on. However, all the surface measurements were conducted after normalizing the surface to account for any tilt of the resin mount. This was done using the 'FormRemoval' function which levels the area of interest. The 3D surface is created using the focus variation microscopy method described in Section 2.4.3. The surface roughness was determined using 5 characteristic lines to be representative of the entire surface, which were averaged to determine the R_a and R_t values. At this stage the areas for cell placement were also chosen based on what was seen as a constant roughness area. Lastly, as a final step before cell deposition the samples were washed again using an ultrasonic bath suspended in ethanol for 5min.

3.2. Cell deposition

A549 cells were cultured in flasks until a specific cell density was reached. In a preliminary test, 5000 cells were planted on each sample. This proved to be a too low cell density, and the cells all appeared dead as observed by their circular shape. For the following tests a higher density was chosen 17,000 and 14,000 for the respective experiments. PMMA tubes 10mm diameter, 1.5mm thickness, and 10mm height were attached to the areas of interest on the metallic samples using a double-sided tape. The samples, and tubes were all rinsed with 70% ethanol. The cells were lifted from the flask into the suspension using trypsin which is an enzyme that cleaves focal adhesion points thus removing surface adhesion [26]. The cells were centrifuged in a Hettich Zentrifugen ROTINA46 at 300g (300 times gravity) for 5min in order to pellet down the cells. Leftover trypsin was aspirated, and the cells were resuspended in cell medium and counted using a hemcytometer. The cells were then deposited into the tubes. Once deposited the cells were incubated for a period of 48 hours to allow for proliferation. The experiments were terminated at 48 hours to prevent over confluence which would result in cell death. The cells were then fixed, i.e. polymerized, using 4% paraformaldehyde and dehydrated using an ethanol series.

3.2.1. Cell density

Table 3 includes the setup for the three experiments that were conducted. The aim of Experiment 1 & 2 was to investigate the cell proliferation on Ti-Grade 2 at various surface roughness values. The goal was to replicate results from literature and determine the optimal surface roughness for cell attachment. The first experiment was preliminary and did not yield positive results, requiring a second iteration. Experiment 3 was focused on determining cell proliferation based on the composition of the metal samples and would support the goal of establishing milled surfaces as appropriate for cell culturing tests. The cell density was calculated using a hemocytometer, which relies on visual cell counting at the four corners of the dish [37].

Table 3: *Cell quantity and description of experiment for the 3 trials*

Experiment	Goal	Number of cells	Goal achieved
1	Determine effects of surface roughness on cell proliferation	5000	N
2	Determine effects of surface roughness on cell proliferation	17000	Y
3	Determine cell proliferation on machined surfaces	14000	Y

The cell quantity was increased from 5000 to 17000 cells because the first experiment resulted in inconclusive results. For the later experiment with the machined surfaces 14000 cells was selected because of the confluence that occurred after 48h of incubation of the previous samples in Experiment 2. This would allow for actual proliferation to be seen with a lower risk for confluence.

3.2.2. Cell fixation

The cell fixation process consists of 3 major steps, rinsing, fixation, and dehydration. Firstly, the cells had to be rinsed in phosphate buffered saline (PBS) twice. This is done to clean off any dead cells, or ones that weren't attached to the surface, and to remove proteins shed from cells and from the medium. Secondly, the remaining cells were fixed during a 15min exposure to 4% paraformaldehyde, which polymerizes them by cross-linking some of the molecules in the cells. This step is similar to other experiments and is used as a standard fixation process [12]. Lastly, the fixed cells had to be dehydrated through an ethanol series of varying ethanol concentrations by replacing water with EtOH. The ethanol dehydration series consisted of the following steps, 30%, 50%, 70%, 90%, 95%. The ethanol solution was left inside the tubes for 15 min, and the last step of 95% ethanol was left until it fully evaporated. This is done to prevent the cells from changing geometry during dehydration and allow for better cell morphology.

3.3. Quantification

In order to determine the amount of proliferation the cells have to be counted. In order to count the cells a SEM is utilized since the metal surfaces are not

transparent which is the preferred method of counting cells in cell culturing experiments. To prepare the samples for SEM, the cells had to be sputter coated with metal in order to reduce the charging of the sample and allow for image resolution. Once the cells are able to be visualized, they had to be counted. To aid in cell counting, images were taken with a field of view of, 200 µm, 1mm, and 2mm. The images were then used to determine the area density of the cells based on image analysis techniques as described later.

3.3.1. Au/Pd sputtering

BALZERS SCD004 was used to sputter coat the metal sample surfaces, and the attached cells. The sputtering was done with chamber pressure $7x10^{-2}$ mbar, and a current of 15mA, for 250 seconds. The steps followed were provided with the machine and supplied a coating of Au/Pd of above 15nm.

3.3.2. SEM

A MIRA3 TESCANN scanning electron microscope was used after the samples were sputtered to allow for the counting of cells and investigating the type of attachment. Most of the analysis was performed at 15kV, however for samples where an oxidized layer was present (AZ31, and AZ61a) the accelerating voltage was increased to 20kV. The characteristic sample field view was at 1 or 2mm which allowed for cell counting. The cell counting was performed using image analysis techniques, which are described in more detail in the following sub-section. The 2mm area was imaged and chosen as a characteristic area which is representative of the entire sample.

3.3.3. Cell volume density

Cell area density was calculated using image analysis techniques. The images were already black and white (BW) which allowed them to be evaluated using a grey scale. A grey scale is simply the variation of intensity ranging from white to black. The written code imports the BSE image into the workspace and plots a histogram which counts the number of cells at the different values of the grey scale. This histogram represents the color distribution in the image and can be seen in Figure 7 (b). The area fraction is determined numerically by dividing the number of pixels above the present grey scale limit by the total number of pixels present in the image. The threshold for the grey scale values was determined by using the 'colorThresholder' app in Matlab. The limit was set based on the visual inspection of the image, and this threshold was kept constant for all

specimens. Figure 7 (a) shows the masked BSE image where the cells above the threshold are highlighted in blue. Appendix D - Image processing Matlab code provides the Matlab code used.

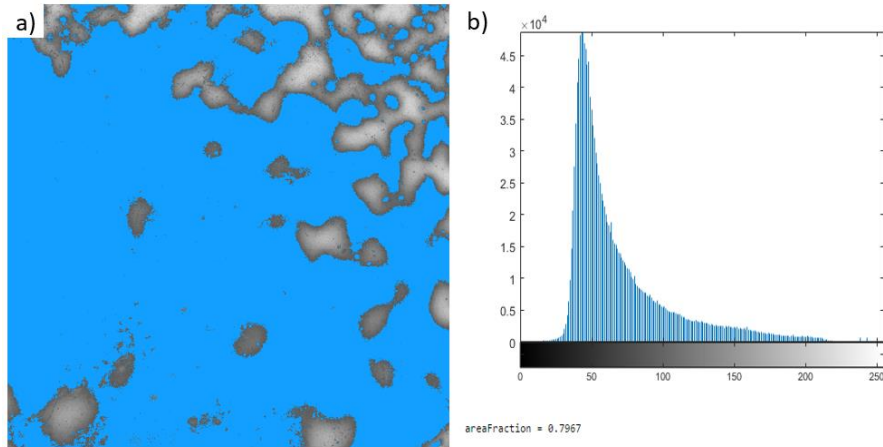*Figure 7: Matlab script results; 'colorThresholder' result (a), sample result from grey scale image (b)*

3.3.4. Categorization

The cells are then categorized based on the number of cells still present and compared to the glass slide sample which was used as a reference. Lastly, the cells are also categorized with the type of cell attachment; circular, or spread-out resulting in a more elongated/amorphous shape.

4. Results & Discussion

This section contains the results obtained from testing, and the supporting discussions. The three main sections are regarding; achieving specific surface roughness, tool wear of the milling insert, and cell proliferation.

4.1. Targeting specific surface roughness

This section focuses on developing a model for targeting specific surface roughness. Firstly, the samples had to be hardness tested in order to determine the appropriate settings for the grinding machine. Secondly, the surface roughness of the selected materials was determined after grinding based on R_a and R_t values obtained from the 3D optical microscope.

4.1.1. Hardness testing

Hardness is one of the components of the machinability polar diagram that is outlined in the book by Ståhl *et al*. Hardness is further described as not a measure of machinability, but rather the resistance to surface plastic deformation [21]. Since grinding relies on plastic deformation in order to cut the sample, the material hardness would have an impact on the time and force required to machine. Hardness testing was necessary to determine the specifications for grinding that were used later in the experiment for sample preparation. Effects of hardness were also seen in the slope of the developed trends during the grinding process. This can be clearly seen in Figure 9 where harder materials developed a more pronounced logarithmic trendline. Table 4 provides the hardness values for the selected material samples. The values for hardness are given on the Vickers scale, and were averaged using 5 measurements for each sample.

***Table 4:** Vickers hardness values of the samples*

Sample	Vickers Hardness
Ti6Al4V	309,96
AZ31	57,9
AZ61a	72,54
Al 7075	174,74
CW510L	155,78
Ti Grade 2	253,54

4.1.2. Developing a model

Originally Ti Grade 2 was used for targeted surface roughness. All other samples were grinded through the entire process to achieve the smallest surface roughness possible. For Ti Grade 2 the target roughness was estimated based on the grit size of the papers. During optical microscopy however, it was concluded that the grit of the SiC paper does not correspond to the surface roughness achieved. As a result, the various samples that were prepared using the different grit sizes of; P220, P500, P1200, P2000, and P4000 yielded different surface roughness values but nowhere near the expected results. This led to the development of a model that would allow for the achievement of targeted surface roughness.

The obtained surface roughness values for both R_a and R_t were recorded and can be seen in Figure 8. A decline in surface roughness can be seen when finer grit SiC paper is used. This follows the logic that with a finer grit the surface roughness would be less. The general trend that the lines seem to follow, is that with a finer grit size the surface roughness values change at a smaller rate. This leads to an eventual plateau, when SiC paper is no longer an option, and diamond suspension polishing starts. This study focused on only grinding operations, as a result the area that was investigated was between SiC grit size of P220 and up to P4000.
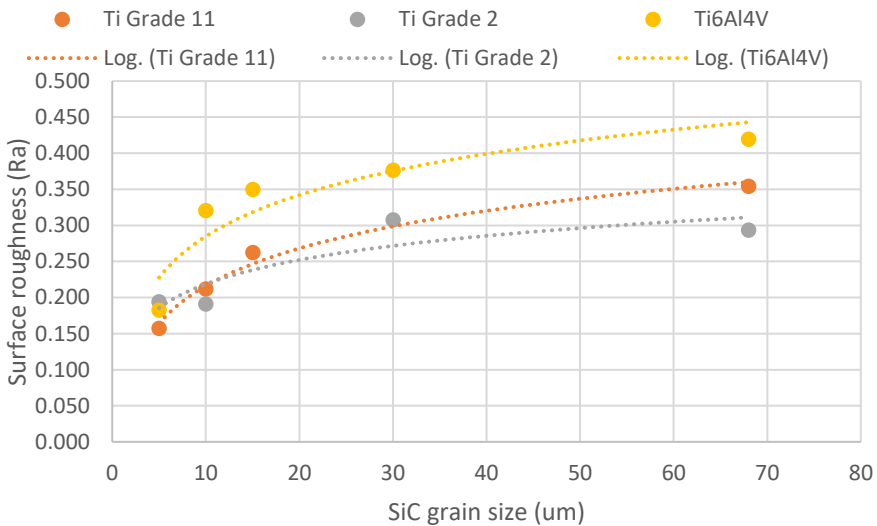

Figure 8: *Identifying surface roughness trends based on the SiC sandpaper grain size used for grinding*

4.1.3. Model testing

Figure 9 illustrates the recorded R_a values for AZ31, AZ61a, CW510L, and Al 7075 and their respective SiC grain size. The difference in the achieved surface roughness R_a values being larger is due to the scarcity of P220 grinding paper at the lab. Unfortunately, when the experiments were conducted there was no P220 grinding paper which is the roughest. Therefore, the amount of material removed is less and the final achieved surface roughness at the different stages is less than previously shown in Figure 8.
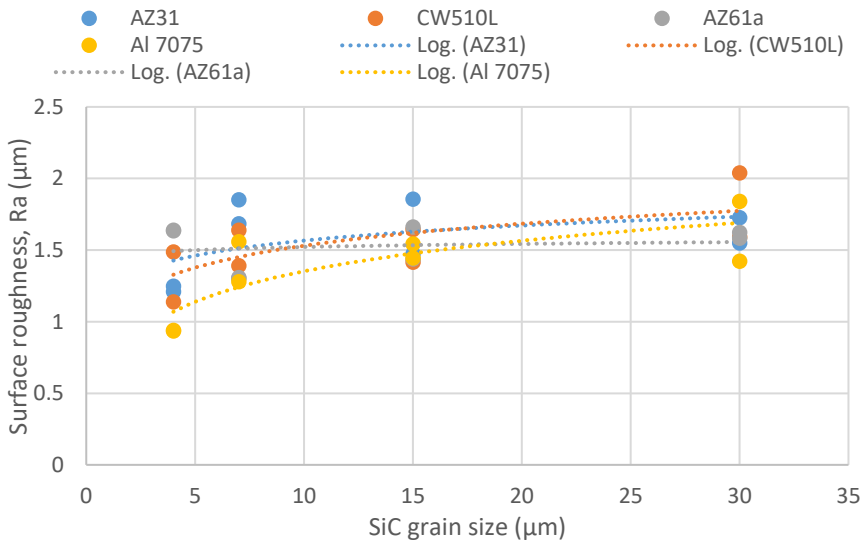
Figure 9: *Surface roughness trends used for determining a theoretical model to compare with future results*

The logarithmic trendline seems to be consistent across all samples as seen in Figure 9. In order to speed up future processes an equation line was created for each sample based on the grain size of SiC paper used and the achieved surface roughness. The trendline was designed using a logarithmic trendline setup to allow for the best fit. The logarithmic trendline equation was calculated in Excel and used for determining the theoretical value at each grain size value the equations can be found in Appendix E - Theoretical logarithmic trendline equations for surface roughness targeting. The next step in developing this model is to test it.

The model was tested by conducting the grinding steps one more time for each material sample. The achieved surface roughness (R_a) value at each stage of grinding was compared with the theoretical value obtained from the logarithmic trend. The samples were grinded with the same procedure and the process was terminated at 30, 15, 7, and 4 µm grain size grinding paper steps. This was done to determine the percent error that was present when compared to the original trendlines. Table 5 shows the percentage error when compared to the values of R_a for the theoretical points using the developed trendline equation.

Table 5: *Percent error values for the experimentally obtained surface roughness R_a values for AZ31, CW510L, AZ61a, and Al 7075*

Material	FEPA P scale	Grain size (µm)	Percent error (%)
AZ31	P500	30	0,2
	P1200	15	0,2
	P2000	7	6,4
	P4000	4	2,8
CW510L	P500	30	5,6
	P1200	15	10,6
	P2000	7	9,9
	P4000	4	4,5
AZ61a	P500	30	3,1
	P1200	15	3,3
	P2000	7	2,2
	P4000	4	4,9
Al 7075	P500	30	5,1
	P1200	15	0,6
	P2000	7	9,3
	P4000	4	12,6

The percent error values that exceeded 5% were highlighted in yellow. It can be seen that both Mg-alloys performed well when compared to the theoretical trendline. CW510L, and Al 7075 both have a higher hardness value this could be the result of the higher difference in percent error values. Since R_a is based on an arithmetic mean deviation they are influenced by large Rt values. All the samples exhibited larger Rt values ranging up to 12 µm. This is the result of the inability to grind with P220 grinding paper. A possible solution would be to grind for longer times. Overall, grinding operations are

conducted in steps therefore the original surface roughness plays a large role in determining how much pre-defined steps will aid in reducing the R_a value.

4.2. Milling tool wear

For the second part of the experiment samples were prepared using a milling process. The only limiting factor for utilizing a machining process is the wear that occurs on the tools, which leads to the need for tool replacement.
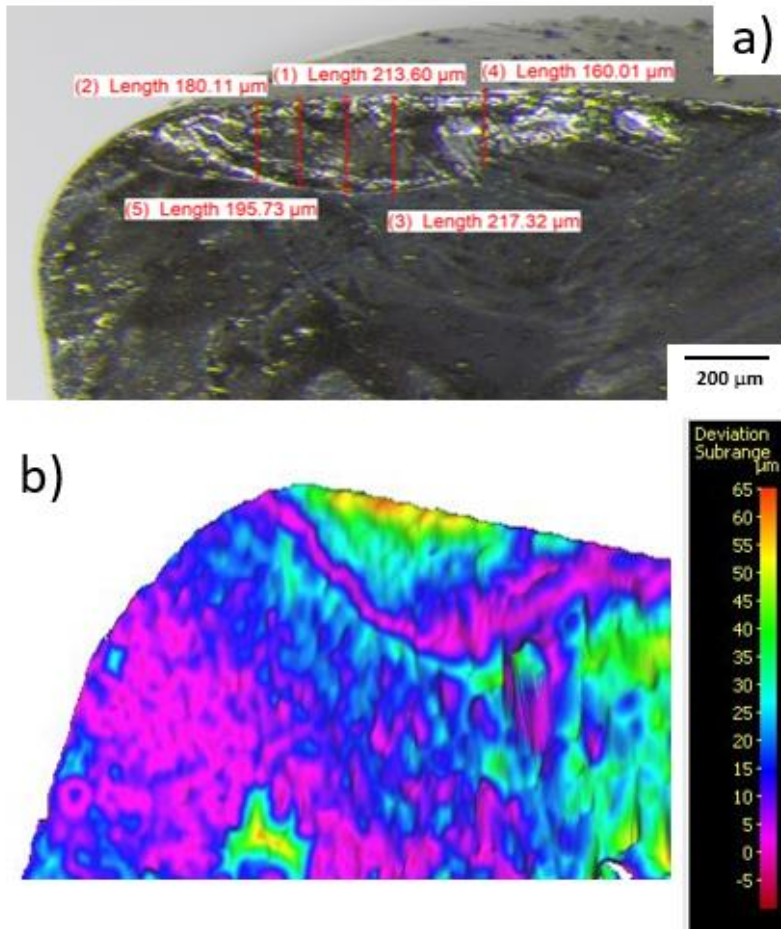

Figure 10: Showing the crater and flank wear experienced by the milling tool insert. The measured VB values (a), and the volume difference measurement performed with a 3D microscope (b)

Figure 10 shows the wear that is present on the milling tool that was used in sample preparation. The most visible wear that occurred was crater wear which was most likely the result of abrasive and adhesive wear during the cutting process. The adhesive wear can be clearly seen due to the chipping on the rake face. Based on literature this was most likely due to high temperatures experienced by the tool insert during the cutting operation [21]. This could be the result of either not utilizing cutting fluid, or improper cutting conditions. Since the same cutting data was used for all samples to allow for consistency it is most likely the combination of improper cutting data, and the lack of cutting fluid to aid in cooling of the cutting zone. The tool life criterion is defined as when a tool is no longer able to be used to achieve the same mechanical properties or quality specifications [21]. This can be seen in the increasing values for R_a with the later samples like CW510L that resulted in a surface roughness of 0.404 µm. This suggests that both the tool was wearing out, and that perhaps the cutting conditions could be modified to fit the machining process better. Ideally a range of experiments would be conducted to both develop a wear model for machining individual metals and determine the appropriate cutting conditions for achieving specific surface roughness values.

By utilizing a simple machining process of milling the time for sample preparation and optical inspection can be reduced drastically. There are many surface roughness equations that rely on the cutting data used to determine the final surface properties. These equations could further aid in determining the appropriate cutting data. With the following cutting data of feed (f) 55 mm/min, and nose radius (r) of the tool which was 0.2 mm a range of R_a values was achieved. The optimal surface roughness of approximately 0.15 µm as defined in [11] was achieved by Al 7075, and Ti6Al4V.

4.3. Cell proliferation

This section outlines the results obtained with regards to the cell proliferation on the various metallic samples. These were considered both from the physical perspective of varying surface roughness, and for determining whether machined surface preparation is enough for cell proliferation experiments.

4.3.1. Surface roughness variation

As previously described some literature found that cells preferred a rougher surface, and there was also supporting literature for smoother surface cell

proliferation. This led to the idea that perhaps cell proliferation occurs within an optimal range. Below or above that range the number of cells that remain attached decreases, graphically this would be perceived as a U-shaped curve. The investigated samples used for surface roughness was Ti Grade 2 and Ti Grade 11. The goal was to determine which surfaces had the most cell attachment.

The SEM was used with an accelerating voltage of 15kV for all samples within the surface roughness experiment. This was due to the fact that no oxidization was present on the surface and the image was sharpest at these settings. If the acceleration voltage was to be increased the penetration depth would also increase and the surface qualities would become more blurred. This was utilized for samples with an oxidized layer present on the surface. The spot size was 5nm. Increasing the spot size and beam intensity would allow more electrons through to the surface resulting in potentially more reflections and charging the surface which would lead to a blurry image. Firstly, it is important to identify the cells. This was done by utilizing XEDS techniques which helps identify the composition of the sample. The provided plots can be overlaid on top of BSE images in order to identify the features that correspond to the cells. Since the cells are carbon based, searching for carbon locations through XEDS will help identify the cells. From XEDS, the carbon concentrations in Figure 11 show the areas for high cell densities.
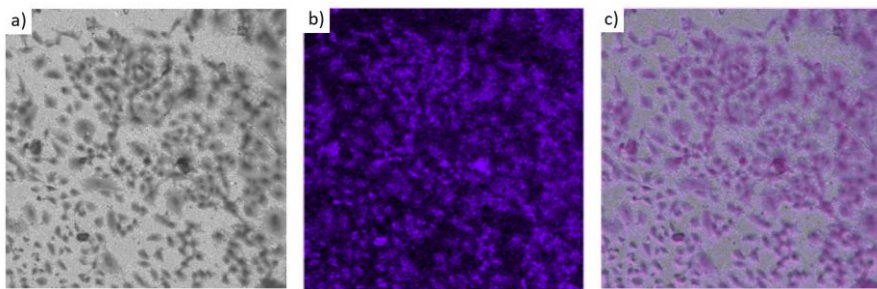

Figure 11: Overlaid image of carbon concentrations (c) BSE image of Al 7075 (a), and the XEDS results for carbon (b)

Figure 12 shows the BSE images for the Ti Grade 2 sample as an example of results. The images were taken for 4 different surface roughness values which were named based on their R_a values 0.158, 0.212, 0.263, and 0.354 µm respectively.
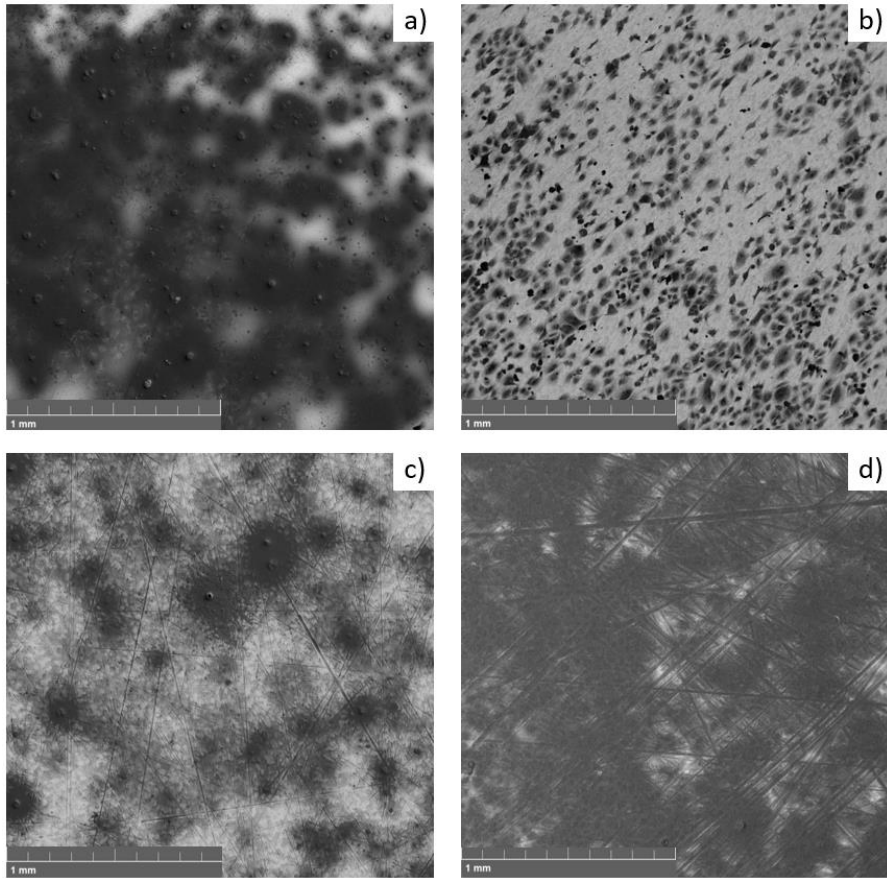
Figure 12: *SEM images of the Ti Grade 2 sample using BSE imaging at the various surface roughness specifications; 0.158 µm (a), 0.212 µm (b), 0.263 µm (c), and 0.354 µm (d)*

Based on visual observations it can be seen that the cells are most clearly seen in Figure 12 (b). This is most likely due to the density of the cells. For most other images a pooling of cells can be witnessed which suggests that the density is much higher. However, it is also possible that the SEM settings were not optimal for the image taken. Since all results could benefit from reproducibility, that would be the suggestion for further work.

***Table 6: Surface roughness and the obtained area fractions (AF) based on
the image analysis from Matlab***

Sample	Ra (µm)	AF
Ti Grade 2	0,158	0,7967
	0,212	0,2066
	0,263	0,2756
	0,354	0,5438
Ti Grade 11	0,194	0,4781
	0,294	0,5377
Glass (Ref.)	-	0,3151

To support the previously discussed U-shaped trend it is necessary to plot
the Table 6 results. From Figure 13 it can be seen that the U-shaped trend
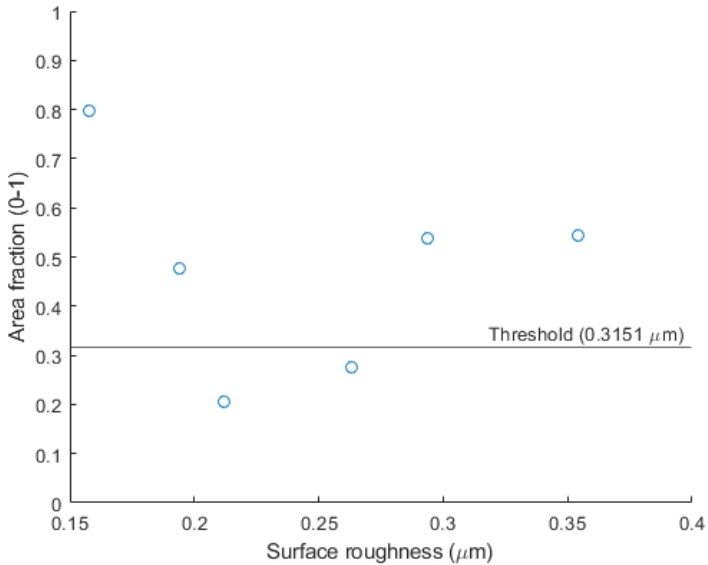does indeed occur for the various surface roughness values.

Figure 13: *Area fraction graphical representation for the Ti Grade 2 and
Ti Grade 11 samples, with the 'Threshold' value from the Glass (reference)*

Figure 13 shows that the area fractions for the smoother and rougher surface roughness values are above the threshold. In this case the threshold value is based on the cell proliferation on glass slides which were used as a reference of current methods. The U-shaped curve is not clearly visible, however as previously mentioned by Huang *et al.* the most cell proliferation was seen around a surface roughness of 0.15 µm [11]. Additionally, the rougher end of the spectrum shows an increase in cell proliferation as well which suggest the possibility for a U-shaped trend. This increase in cell proliferation with increased surface roughness was observed by Keller *et al.* [10]. A further investigation with a larger range of surface roughness values would be beneficial to determine whether 0.15 µm is a local maximum as suggested previously. Chung *et al.* concluded that on a nano-scale an increase in surface roughness leads to more cell proliferation and better cell adhesion [3]. This would suggest that inversely from the 0.15 µm surface roughness the cell proliferation and adhesion should decrease. Or if this increase in cell proliferation continues increasing with reduced surface roughness as suggested by [2]. Since the literature related trends were observed in this method testing experiment, it is valid to assume method correctness.
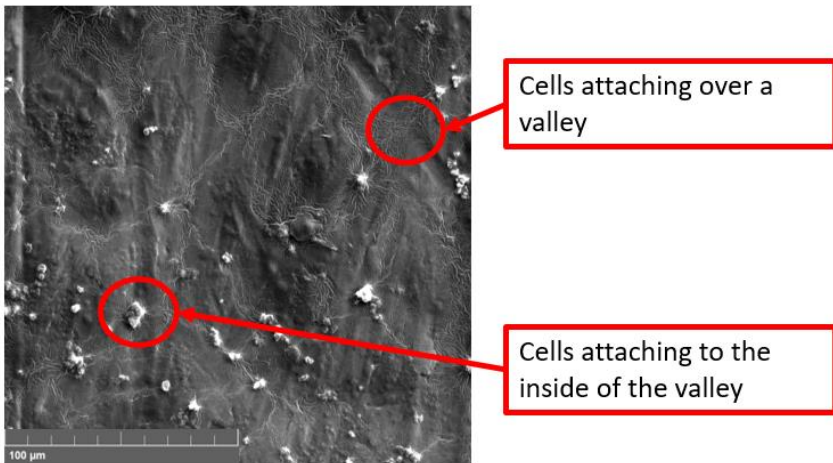

Figure 14: Cell attachment properties showing two types of attachment

Diving a bit deeper, at a closer look a trend can be seen that some cells bridged over the rough valleys, and some attached within the valleys. Figure 14 shows the different cell placements through a SE image. Due to the circular grinding process, the peaks and valleys do not follow a parallel

pattern. As a result, some cells can be seen bridging over the grinded valleys, and some placing themselves within the valleys. It would be interesting to further determine whether the cells have a preference as described in [12]. Additionally, it would be interesting to investigate if cell proliferation happens directionally based on the roughness of the surface as suggested in [11]. This could be done by creating control sample groups with unidirectional grinding procedures, and one with an amorphous pattern achieved through circular grinding.

4.3.2. Machined surface analysis

The machined samples were all milled with the goal to have a uniform surface developed regardless of the metal composition. This section would focus more on two main issues the possibility of cell proliferation experiments on easily machined surfaces, and the chemical effects of composition on the preferred cell proliferation areas. Lastly, a classification system was developed to rank the materials against each other in cell density, and cell attachment.

The goal of classifying the cells into specific groups is to identify which samples performed best in terms of cell density, and whether cells attached. The first is easy since it is a direct result of the area fractions that were computed through image analysis similar to the method in the previous section. The latter, however, is harder to quantitively determine. To determine whether the cells attached and were thriving in the metal conditions the shape and surrounding areas around the cells were analyzed. Firstly, if the cells were adhered and thriving the areas around the cells would be a lighter shade of grey with carbon deposits which would be the result of the cells spreading and adhering on a larger area. Secondly, the actual shape of the cells can be used to determine if the cells deemed the surface as toxic, or uninhabitable. If the cells were more circular in shape, they were in an environment that is not as prosperous when compared to cells that were of a more elongated/amorphous shape.

Table 7: *Area fraction results for the milled metallic samples*

Sample	Ra (µm)	AF
Ti6Al4V	0,165	0,4281
AZ31	0,285	0,3748
CW510L	0,404	0,2244
Al 7075	0,146	0,4023
Glass (ref)	-	0,3364

Table 7 shows the tabulated values based on the image analysis to determine the area fraction of cells present on the sample surfaces. Similarly, the results from cell proliferation on the glass slides was used as a measure of reference and set as a threshold value. Figure 15 illustrates the obtained cell proliferation values for the milled metal samples compared to the glass slide values shown as a reference threshold.
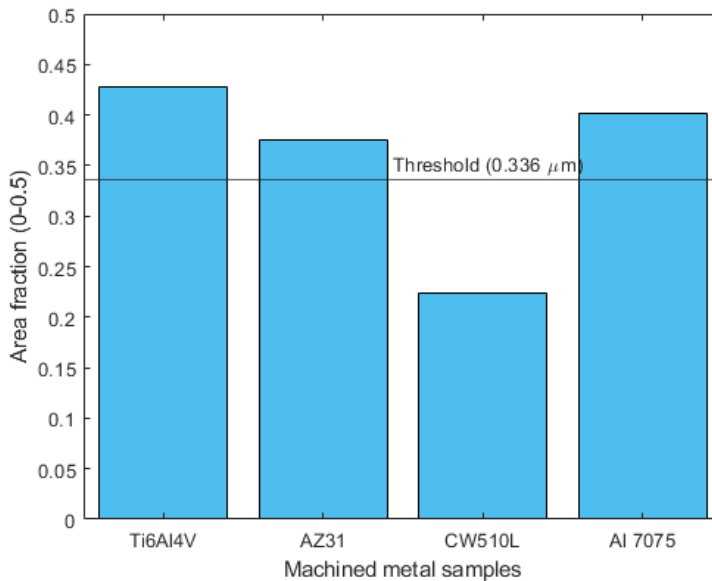

Figure 15: *Area fraction values for cell proliferation for the milled metal samples compared to the threshold value of 0.336 µm*

Figure 16 (b) shows the brass sample which consists of copper-rich environments which are known to be toxic to cells, the cells remained in circular shapes and did not spread out. In other words, the cells did not see copper-rich environments as an inhabitable environment. This is consistent with previous research [4, 5, 8], however a preferred attachment site can be seen. An XEDS spot analysis would be beneficial in order to determine if the less copper-rich surface was the one with higher cell attachment. Unfortunately, due to time constraints the XEDS spot analysis was not done.
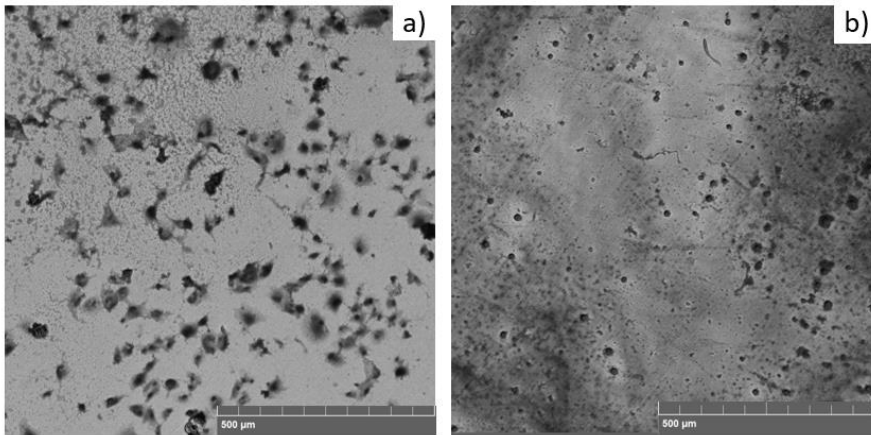
Figure 16: BSE images of different cell attachment types; (a) amorphous cell spreading on Ti6Al4V, (b) circular cell spreading on Brass

Figure 16 (a) shows the Ti6Al4V sample and the cells in their elongated/amorphous shape with light grey areas around meaning that the cells are able to proliferate in this environment. It is a viable sample preparation surface to sustain cell proliferation experiments. Table 8 shows the ranking of the different samples based on the viability of the environment and cell shape from visual inspection. This aims at helping future studies with determining which metals can be used for cell proliferation experiments and highlighting the ones with potential for use in the implant industry.

Table 8: Cell attachment type, used to determine the viability of the environment which is characteristic of the chemical properties of the metal sample

Sample	Cell attachment type
7075 Al	Amorphous
AZ31	Slightly amorphous
CW510L	Circular
Ti6Al4V	Amorphous

The two Mg-alloys, however, are not comparable since AZ61a oxidized heavily and did not produce any quantifiable results because the cells were simply not visible. However, based on literature it was expected that AZ61a would perform worse than AZ31 due to its higher Si content as described in [20]. Although the density for AZ31 was comparable to that of Al 7075, the shape of the cells present on the surface was only slightly amorphous. This suggests that the cells found the surface less desirable, however this could also be the result of surface roughness which was almost twice as rough as the Al 7075 sample. When compared to the glass slide threshold limit the AZ31actually performed better, but the deviation is too low to consider these results conclusive.

Based on the results obtained it is reasonable to say that machined surfaces can be used for cell proliferation experiments. All the samples except for CW510L performed better than the glass slide threshold, which suggests that for future experimentation it would be beneficial to directly plant the cells on metallic surfaces. This would allow for further development of the understanding of cell and metal interactions. Simple machining operations such as milling have shown good results without any noticeable hindering of cell proliferation. This opens the door for future experimentation with reduced sample preparation times and a well-defined workflow for cell proliferation testing on metal samples.

4.3.3. Oxidized samples

The AZ61a sample had severe oxidation which can be seen in Figure 17. Since the oxidation was severe and not characteristic of magnesium alloys, this was concluded to be the result of contamination. The dendritic structures are most likely present from the saline solution and are salt crystals. A study by Schwarz *et al.* achieved similar structures and classified them as salt particles. Although the study was on a different topic, it was used in order to identify salt particles in the SEM image [38]. These salt crystals are the remnants of the (PBS) saline solution which much have remained on the surface and reacted with the magnesium below the oxide layer. Unfortunately, they were not removed during the EtOH dehydration series. The main MgO oxide layer underneath seems to have morphed into this wool-shaped layer, which suggests something triggered expansion/growth from below the oxide layer. This was most likely due to a chemical reaction between the F-12K medium used for cell culturing and the core metal components. The medium was also seen to have changed color which generally symbolizes a change in the pH value.
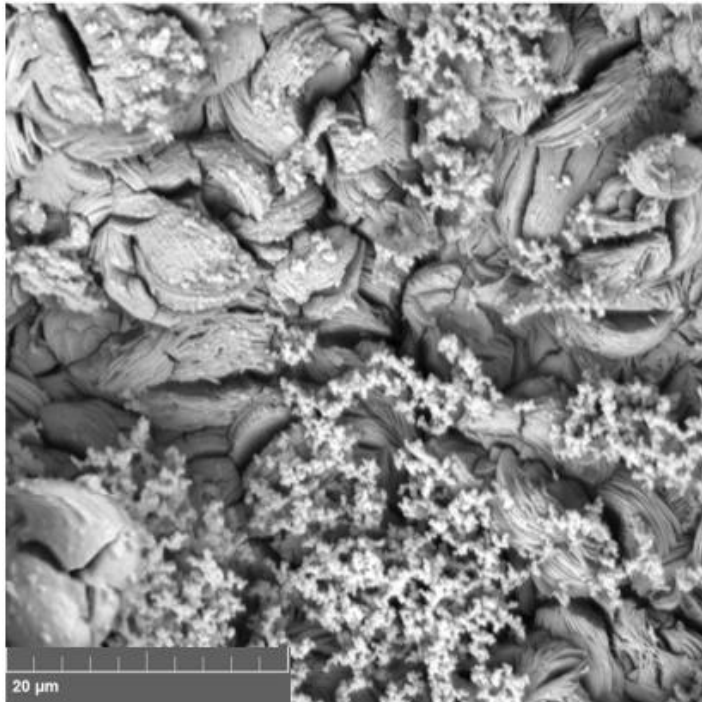

Figure 17: *Oxidized ASTM B-107 sample more commonly known as AZ61a*

5. Conclusions

The results from the surface roughness variation experiment were consistent with currently known literature. The amount of cell proliferation was noticeably higher at the smoother and rougher ends of the spectrum. With the highest cell proliferation seen through area fraction image analysis at approximately 0.15 µm. The two lowest cell proliferation results were seen in the middle range of surface roughness values at 0.212, and 0.263 µm. Both of these results were also below the control sample (glass slide reference) value of 0.3151 µm.

The metallic samples that were milled using the provided tool insert were analyzed and compared to a glass slide reference as well. All the samples (AZ31, Al 7075, and Ti6Al4V) except for Cu-alloy (CW510L) were above the threshold value of 0.3364 µm. This suggests that the three metal alloys are viable test subjects for further experimentation. Leading to potential use in the implant industry.

The attachment of the cells was also analyzed visually through cell shape, namely a circular shape signifying poor proliferation conditions, and an elongated/amorphous shape symbolizing good proliferation conditions. Ti6Al4V and Al 7075 showed clear amorphous shapes meaning the cell thrived on those surfaces. AZ31 was considered 'slightly amorphous' which meant that some of the cells looked circular, while most exhibited an amorphous shape. This suggests that AZ31 would have to be researched further in order to determine if the results are accurate or if there is something hindering cell proliferation. Lastly, CW510L was seen to only contain circular shaped cells which meant poor proliferation conditions, which was expected based on previous literature.

Finally, AZ61a did not yield any conclusive results due to a heavily oxidized layer. Due to this no observations were made with regards to cell proliferation, shape, or attachment properties.

6. Further work

The ever-growing field of material science yields new alloys constantly, which results in the need for more testing to understand the future biocompatibility of those metals. The surface roughness study would benefit from more test points, which would mean repeating the experimental procedure to allow for a better statistical representation.

The overall trend of surface roughness effects on cell proliferation should be extended to include a wider range of surface roughness values. This would allow for the investigation of cell proliferation behavior at rougher surfaces and finer surfaces to conclude whether the previously known trends are consistent for the entire range or only within the investigated ranges. Since cell proliferation is expected to start decreasing below 0.15 µm and continue increasing at the other end of the investigated range. This would suggest that a local maximum does exist around the 0.15 µm surface roughness. This would be something not previously concluded by any author.

Reproducibility of results obtained with the milled metal samples should be further investigated to prove the validity of drawn conclusions. Including a more diverse range of metal alloys would also help the overall understanding of the effects of alloying on the cell proliferation. This would aid in determining which alloying combinations result in better cell proliferation, and if more cytotoxic elements can be alloyed to reduce the overall sample cytotoxicity.

Lastly, an investigation into cell proliferation directionality was mentioned in literature but it was never the core aim of these studies. Surface roughness is the result of investigating the valleys and peaks present within the material. It would be beneficial to investigate the proportionality between the cells attaching within the material valleys and the ones bridging them, and whether there is a preference at the different surface roughness values.

References

[1]   B. Boyan, "Role of material surfaces in regulating bone and cartilage cell response," *Biomaterials,* vol. 17, no. 2, pp. 137-146, 1996-01-01 1996, doi: 10.1016/0142-9612(96)85758-9.

[2]   K. Anselme *et al.*, "The relative influence of the topography and chemistry of TiAl6V4 surfaces on osteoblastic cell behaviour," *Biomaterials,* vol. 21, no. 15, pp. 1567-1577, 2000-08-01 2000, doi: 10.1016/s0142-9612(00)00042-9.

[3]   T.-W. Chung, D.-Z. Liu, S.-Y. Wang, and S.-S. Wang, "Enhancement of the growth of human endothelial cells by surface roughness at nanometer scale," *Biomaterials,* vol. 24, no. 25, pp. 4655-4661, 2003-11-01 2003, doi: 10.1016/s0142-9612(03)00361-2.

[4]   R. G. Craig and C. T. Hanks, "Cytotoxicity of Experimental Casting Alloys Evaluated by Cell Culture Tests," *Journal of Dental Research,* vol. 69, no. 8, pp. 1539-1542, 1990-08-01 1990, doi: 10.1177/00220345900690081801.

[5]   V. Grill *et al.*, "The influence of dental metal alloys on cell proliferation and fibronectin arrangement in human fibroblast cultures," *Archives of Oral Biology,* vol. 42, no. 9, pp. 641-647, 1997-09-01 1997, doi: 10.1016/s0003-9969(97)00055-1.

[6]   Y. Shin and M. Akao, "Tissue Reactions to Various Percutaneous Materials with Different Surface Properties and Structures," *Artificial Organs,* vol. 21, no. 9, pp. 995-1001, 2008-11-12 2008, doi: 10.1111/j.1525-1594.1997.tb00514.x.

[7]   A. S. G. Curtis and C. D. W. Wilkinson, "Reactions of cells to topography," *Journal of Biomaterials Science, Polymer Edition,* vol. 9, no. 12, pp. 1313-1329, 1998-01-01 1998, doi: 10.1163/156856298x00415.

[8]   D. Brune, "Metal release from dental biomaterials," *Biomaterials,* vol. 7, no. 3, pp. 163-175, 1986-05-01 1986, doi: 10.1016/0142-9612(86)90097-9.

[9]   J. L. Woodman, J. J. Jacobs, J. O. Galante, and R. M. Urban, "Metal ion release from titanium-based prosthetic segmental replacements of long bones in baboons: A long-term study," *Journal of Orthopaedic Research,* vol. 1, no. 4, pp. 421-430, 1983-01-01 1983, doi: 10.1002/jor.1100010411.

[10]   J. C. Keller, "Tissue Compatibility to Different Surfaces of Dental Implants: In Vitro Studies," *Implant Dentistry,* vol. 7, no. 4, pp. 331-337, 1998.

[11]   H.-H. Huang, C.-T. Ho, T.-H. Lee, T.-L. Lee, K.-K. Liao, and F.-L. Chen, "Effect of surface roughness of ground titanium on initial cell adhesion," *Biomolecular Engineering,* vol. 21, no. 3-5, pp. 93-97, 2004-11-01 2004, doi: 10.1016/j.bioeng.2004.05.001.

[12]   R. Lange, F. Lüthen, U. Beck, J. Rychly, A. Baumann, and B. Nebe, "Cell-extracellular matrix interaction and physico-chemical characteristics of titanium surfaces depend on the roughness of the material," *Biomolecular Engineering,* vol. 19, no. 2-6, pp. 255-261, 2002-08-01 2002, doi: 10.1016/s1389-0344(02)00047-3.

[13]   X. Wen, X. Wang, and N. Zhang, "Microrough surface of metallic biomaterials: a literature review," *Bio-Medical Materials and Engineering,* vol. 6, no. 3, pp. 173-189, 1996-01-01 1996, doi: 10.3233/bme-1996-6305.

[14]   Struers, *Technical Data*, Struers website, 2020. [Online]. Available: https://publications.struers.com/brochures/english/technical-data-sheet/consumables/sic-foil-paper/?_ga=2.139574899.1513083020.1620058863-848220634.1620058863.

[15]   J. I. Rosales-Leal *et al.*, "Effect of roughness, wettability and morphology of engineered titanium surfaces on osteoblast-like cell adhesion," *Colloids and Surfaces A: Physicochemical and Engineering Aspects,* vol. 365, no. 1-3, pp. 222-229, 2010-08-01 2010, doi: 10.1016/j.colsurfa.2009.12.017.

[16]   A. Pizzoferrato *et al.*, "Cell culture methods for testing Biocompatibility," *Clinical Materials,* vol. 15, no. 3, pp. 173-190, 1994-01-01 1994, doi: 10.1016/0267-6605(94)90081-7.

[17]   D. M. Findlay, K. Welldon, G. J. Atkins, D. W. Howie, A. C. W. Zannettino, and D. Bobyn, "The proliferation and phenotypic expression of human osteoblasts on tantalum metal," *Biomaterials,* vol. 25, no. 12, pp. 2215-2227, 2004-05-01 2004, doi: 10.1016/j.biomaterials.2003.09.005.

[18]   G. Song and S. Song, "A Possible Biodegradable Magnesium Implant Material," *Advanced Engineering Materials,* vol. 9, no. 4, pp. 298-302, 2007-04-01 2007, doi: 10.1002/adem.200600252.

[19]   L. Li, J. Gao, and Y. Wang, "Evaluation of cyto-toxicity and corrosion behavior of alkali-heat-treated magnesium in simulated body fluid," *Surface and Coatings Technology,* vol. 185, no. 1, pp. 92-98, 2004-07-01 2004, doi: 10.1016/j.surfcoat.2004.01.004.

[20]   X. Gu, Y. Zheng, Y. Cheng, S. Zhong, and T. Xi, "In vitro corrosion and biocompatibility of binary magnesium alloys," *Biomaterials,* vol. 30, no. 4, pp. 484-498, 2009-02-01 2009, doi: 10.1016/j.biomaterials.2008.10.021.

[21]   J.-E. Ståhl, *Metal cutting theories and models*. Seco Tools, AB, 2012.

[22]   *3685*, I. O. f. Standardization, 1993.

[23]   S. Malkin and C. Guo, *Grinding technology: theory and application of machining with abrasives*. Industrial Press Inc., 2008.

[24]   M. A. Corporation, *Quick guide to surface roughness measurement*, USA, 2016, p. 8.

[25]   D. A. Macdonald, "The application of focus variation microscopy for lithic use-wear quantification," *Journal of Archaeological Science,* vol. 48, pp. 26-33, 2014-08-01 2014, doi: 10.1016/j.jas.2013.10.003.

[26]   M. A. H.R.H Patel, I.S. Shergill, *Basic science techniques in clinical practice*, British Library: Springer-Verlag London Limited, 2007.

[27]   D. Cui, F. Tian, C. S. Ozkan, M. Wang, and H. Gao, "Effect of single wall carbon nanotubes on human HEK293 cells," *Toxicology Letters,* vol. 155, no. 1, pp. 73-85, 2005-01-01 2005, doi: 10.1016/j.toxlet.2004.08.015.

[28]   T. Sun, Y. Yan, Y. Zhao, F. Guo, and C. Jiang, "Copper Oxide Nanoparticles Induce Autophagic Cell Death in A549 Cells," *PLoS ONE,* vol. 7, no. 8, p. e43442, 2012-08-20 2012, doi: 10.1371/journal.pone.0043442.

[29]   D. E. N. Joseph I. Goldstein, Joseph R. Michael, Nicholas W.M. Ritchie, John Henry J. Scott, David C. Joy, *Scanning electron microscopy and X-ray microanalysis*. USA: Springer, 2018.

[30]   M. Dewar, "Characterization and Evaluation of Aged 20Cr32Ni1Nb Stainless Steels," Masters, Department of Chemical and Materials Engineering, University of Alberta, 2013.

[31]   G. L. A. Polishetty, V. Manoharan, C. Sonavane, "MACHINABILITY ASSESSMENT OF Ti-6AL-4V FOR AEROSPACE APPLICATIONS," *ASME Early Career Technical Journal,* 2013.

[32]   J. Feliu, Sebastián, A. Samaniego, E. Bermudez, A. El-Hadad, I. Llorente, and J. Galván, "Effect of Native Oxide Film on Commercial Magnesium Alloys Substrates and Carbonate Conversion Coating Growth and Corrosion Resistance," *Materials,* vol. 7, no. 4, pp. 2534-2560, 2014-03-28 2014, doi: 10.3390/ma7042534.

[33]   A. D. Isadare, B. Aremo, M. O. Adeoye, O. J. Olawale, and M. D. Shittu, "Effect of heat treatment on some mechanical properties of 7075 aluminium alloy," *Materials Research,* vol. 16, no. 1, pp. 190-194, 2012-12-04 2012, doi: 10.1590/s1516-14392012005000167.

[34]   A. Toulfatzis, G. Pantazopoulos, C. David, D. Sagris, and A. Paipetis, "Final Heat Treatment as a Possible Solution for the Improvement of Machinability of Pb-Free Brass Alloys," *Metals,* vol. 8, no. 8, p. 575, 2018-07-25 2018, doi: 10.3390/met8080575.

[35]   M. K. Gupta, P. K. Sood, G. Singh, and V. S. Sharma, "Sustainable machining of aerospace material – Ti (grade-2) alloy: Modeling and optimization," *Journal of Cleaner Production,* vol. 147, pp. 614-627, 2017-03-01 2017, doi: 10.1016/j.jclepro.2017.01.133.

[36]   D. G. R. W.D. Callister Jr., *Materials Science and Engineering, An Introduction*, 8th ed. John Wiley & Sons, Inc., 2010.

[37]   M. Absher, "Hemocytometer Counting," in *Tissue Culture*: Elsevier, 1973, pp. 395-397.

[38]   A. D. Schwarz, J. Meyer, and A. Dittler, "Interaction of water droplets with soluble filter cakes in gas cleaning applications," *Separation and Purification Technology,* vol. 259, p. 118128, 2021-03-01 2021, doi: 10.1016/j.seppur.2020.118128.

[39]   A. Seco Tools. "XOEX060204FR-E03 H15." https://www.secotools.com/article/p_00039971 (accessed 03/03, 2021).

Appendix A - Grinding grain size values for FEPA P-scale adapted from [14]

This Appendix shows the adapted values comparing the grain size in µm and tehe FEPA P values for the grinding paper.

Table 9: Grit size comparison obtained from Struers' technical specifications for SiC grinding paper and foil [14]

Grain size (µm)	68	30	15	7	4
FEPA P value	220	500	1200	2000	4000

Appendix B- SECO tool insert

This Appendix provides the specifications found on the SECO tool website with regards to the tool insert used for experiments of the machined surface samples.

| Name	Description	Value
AN	clearance angle major	15.0 deg
Barcode_alt	Alternative barcode	39970000001005
BS	Wiper edge length	1.1 mm
CEDC	cutting edge count	2
CGTT	cutting geometry type technical	E03
CUTINT_SIZESHAPE	insert size and shape	X0.X0602
GAN	insert rake angle	30.6 deg
Grade	Grade	H15
Gradetype	Gradetype	Carbide Uncoated
IH	Insert hand	Right
ItemNumber	Item Number	00039970
LE	cutting edge effective length	6.00 mm
RE	corner radius	0.20 mm
S	Insert thickness	2.45 mm
SSC	Insert seat size code	06
W1	insert width	4.1 mm
Weight	Net weight	0.001 kg
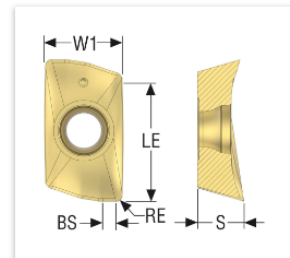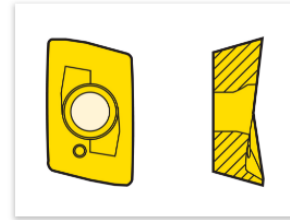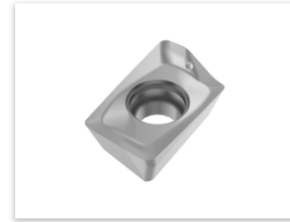
Figure 18: Specifications for the SECO tool insert (XOEX060204FR-E03 H15) as seen on the SECO product website [39]

Appendix C - Grinding conditions for sample preparation

This Appendix has the grinding conditions used for the various metal samples including their setup at the different grinding stages with different SiC grinding disks.

Table 10: Grinding conditions for sample preparation steps of the different metallic samples used

Material	FEPA P value	Force (N)	Time (s)
Ti6Al4V & Ti Grade 2	220	30	45
	500	20	45
	1200	15	60
	2000	10	70
	4000	10	90
AZ31	500	15	30
	1200	10	30
	2000	5	45
	4000	5	45
AZ61a	500	15	30
	1200	10	30
	2000	5	45
	4000	5	45
AL 7075	500	20	40
	1200	15	45
	2000	10	45
	4000	5	60
CW510L	500	10	30
	1200	10	45
	2000	5	45
	4000	5	60

Appendix D - Image processing Matlab code

This Appendix includes the code written in a Matlab Live script format with descriptions of steps.

Image Processing Steps

Used for cell counting through grayscale limits
Import the BSE image obtained from the SEM

```
image = imread(['ImageName.PNG']);
```

Check the grayscale values based on histogram data of the image

```
figure
imhist(image);
```

By using the 'colorThersholder' App within MATLAB a threshold of 90 was selected for the greyscale which masks only the cell related color zone.

```
GreyScaleImage = image > 90;
areaFraction = 1 - sum(GreyScaleImage(:)) / numel(GreyScaleImage)
```

Figure 19: Image processing steps outline in Matlab Live script

Appendix E - Theoretical logarithmic trendline equations for surface roughness targeting

$AZ31, 0.1521 \cdot ln(grain\ size) + 1.2159$ *Equation 2*

$CW510L, 0.2213 \cdot ln(grain\ size) + 1.021$ *Equation 3*

$AZ61a, 0.0313 \cdot ln(grain\ size) + 1.4495$ *Equation 4*

$Al\ 7075, 0.3082 \cdot ln(grain\ size) + 0.6419$ *Equation 5*